research articles Journal of proteome research

An Integrated Metabonomic Approach To Describe Temporal Metabolic Disregulation Induced in the Rat by the Model Hepatotoxin Allyl Formate

Ivan K. S. Yap,[†] T. Andrew Clayton,[†] Huiru Tang,[‡] Jeremy R. Everett,[§] Gilles Hanton,[#] Jean-Pierre Provost,[#] Jean-Loic Le Net,[#] Claude Charuel,[#] John C. Lindon,[†] and Jeremy K. Nicholson*,[†]

Department of Biomolecular Medicine, Division of Surgery, Oncology, Reproductive Biology and Anaesthetics (SORA), Faculty of Medicine, Imperial College London, Sir Alexander Fleming Building, South Kensington, London SW7 2AZ United Kingdom, State Key Laboratory of Magnetic Resonance and Molecular and Atomic Physics, Wuhan Magnetic Resonance Centre, Wuhan Institute of Physics and Mathematics, The Chinese Academy of Sciences, Wuhan, 430071, PR China, Pfizer Global R&D, Ramsgate Road, Sandwich, Kent, CT13 9NJ United Kingdom, and Pfizer Global Research Centre, Amboise, France

Received April 10, 2006

The time-related metabolic events in rat liver, plasma, and urine following hepatotoxic insult with allyl formate (75 mg/kg) were studied using a combination of high-resolution liquid state and magic angle spinning (MAS) nuclear magnetic resonance (NMR) spectroscopic methods together with pattern recognition analysis. The metabonomics results were compared with the results of conventional plasma chemistry and histopathological assessments of liver damage. Various degrees of liver damage were observed in different animals, and this variation was reflected in all of the analyses. Furthermore, each analysis revealed a high degree of functional and structural recovery by the end of the study. The allyl formate-induced changes included hepatocellular necrosis, hepatic lipidosis, decreased liver glycogen and glucose, decreased plasma lipids, increased plasma creatine and tyrosine, increased urinary taurine and creatine, and decreased urinary TCA cycle intermediates. The observed reductions in hepatic glycogen and glucose suggest increased glucose utilization and are consistent with the expected depletion of hepatic ATP following mitochondrial impairment, assuming that there is a consequent increase in energy production from glycolysis. The increase in plasma tyrosine is consistent with impaired protein synthesis, a known consequence of ATP depletion. Partial least squares-based cross-correlation of the variation in the liver and plasma NMR profiles indicated that the allyl formate-induced increase in liver lipids correlated with the decrease in plasma lipids. This suggests disruption in lipid transport from the liver to plasma, which could arise through impaired apolipoprotein synthesis, as with ethionine.

Keywords: Allyl formate • Metabonomics • Metabolomics • Magic Angle Spinning • Nuclear Magnetic Resonance • Liver • Plasma • Urine • Partial Least Squares • Orthogonal-Partial Least Squares • Pattern Recognition

Introduction

Metabonomics offers many opportunities for the study of metabolic perturbation in whole organisms and has been defined as "the quantitative measurement of the multiparametric metabolic response of living systems to pathophysiological stimuli or genetic modification".[1] We and others have shown that this approach can provide valuable information on toxin-induced biochemical perturbations in a variety of biofluids, with metabolic profiles carrying both site- and mechanism-related information, and that the approach can be regarded as complementary to genomics and proteomics approaches.[2−5] The main analytical methods used so far to generate metabonomic (and metabolomic) data in mammalian systems are Nuclear Magnetic Resonance (NMR) spectroscopy and Liquid Chromatography coupled to Mass Spectrometry (LC−MS).[1,2,6,7] Most metabonomic studies have utilized biofluids as noninvasive or minimally invasive reporters of system level biochemical change, but over recent years, the development of high-resolution magic-angle-spinning (HRMAS) as a ^{1}H NMR technique for studying samples of tissues such as liver and kidney has allowed detailed metabolic information to be obtained without tissue disruption, and this has become a

* Correspondence should be addressed to Prof. J. K. Nicholson. E-mail, j.nicholson@imperial.ac.uk; tel., +44 (0)20 7594 3195; fax, +44 (0) 20 7594 3226.

[†] Imperial College London.

[‡] Wuhan Institute of Physics and Mathematics, The Chinese Academy of Sciences.

[§] Pfizer Global R&D, U.K.

[#] Pfizer Global Research Centre, France.

10.1021/pr0601584 CCC: $33.50

Published on Web 09/14/2006

useful adjunct to biofluid NMR studies.[8−11] MAS NMR involves rapid spinning of the sample (typically at 4−6 kHz) about an axis with an angle of 54.7° relative to the applied magnetic field, thus, reducing the line broadening effects from magnetic field inhomogeneity, chemical shift anisotropy, residual dipolar couplings, and sample heterogeneity.[12] MAS NMR spectroscopy is a nondestructive technique requiring small amounts of sample (ca. 8−12 mg) and minimal sample preparation.[13] High-resolution ^{1}H MAS NMR spectroscopy has been successfully applied in the study of biological samples such as liver, kidney, intestine, cardiac tissue, human prostate, and human breast tissue.[14−19] Pattern recognition methods enable the convenient visualization of spectral changes in NMR data and are useful for the detection of specific biomarkers of toxicity and for disease diagnosis.[20−22] Such multivariate analysis can also be used to visualize inherent clustering behavior for organ-specific toxins according to their toxic mechanism. The ability to monitor many compartments using metabolic profiling of biofluids and tissues has allowed us to cross-relate system level reporters during the development of organ failure caused by toxins.[15,17] Here, we apply this integrated approach in a study of the effects of a model periportal hepatotoxin, allyl formate. Furthermore, we report an advance on previous data integration procedures for system level biochemical information recovery in which metabolic profiles from liver and plasma samples taken at the same time are statistically correlated with one another by means of partial least squares (PLS).

Materials and Methods

In-Life Study. All studies were conducted in accordance to the requirements of the relevant national legislation and local guidelines. Twenty male Sprague−Dawley rats (250 g, Charles River, St. Germain-sur-l'Abresle, France) were acclimatized in individual metabolic cages with free access to water and a standard rodent diet (diet A04C, Usine d'Alimentation Rationnelle, Villemoisson-sur-Orge, France). On day 1, 10 of the 20 rats were injected intraperitoneally with 75 mg/kg of allyl formate (AF) in saline, while the other 10 were injected intraperitoneally with saline only. Five animals of each treatment group were euthanized using CO_2 at day 2 and the remainder at day 8. Individual pre- and post-dose urine samples were collected into ice-cooled vessels containing sodium azide (0.1 mL of a 100 mg/mL solution) for 7 h daily with an additional overnight urine collection following the initial 7 h collection on the day of dosing. Individual blood samples were taken under isoflurane anaesthesia from the orbital sinus, immediately prior to euthanasia. These were collected into standard vials containing heparin as an anticoagulant, and the plasma was separated by centrifugation.

Necropsy and Histopathology. Necropsy was carried out immediately after euthanasia. The liver was weighed, and duplicate samples (ca. 20 mg each) of the left liver lobe were immediately snap-frozen in liquid nitrogen and stored for subsequent NMR analysis. The remaining liver tissues were fixed and embedded in paraffin wax, sectioned (4−6 μm), and stained with hematoxylin and eosin for histopathological assessment. Selected liver samples were also stained with Oil Red O and using the Periodic Acid-Schiff (PAS) method to reveal lipid and glycogen deposition patterns, respectively.[23−25]

Clinical Chemistry. Clinical chemistry was carried on a Monarch 200 centrifugal analyzer (Instrumentation Laboratory, Warrington, U.K.). The plasma parameters urea, glucose, total bile acids (TBA), total cholesterol, triglycerides, albumin, total protein (TP), bilirubin, alkaline phosphatase, aspartate aminotransferase (AST), alanine aminotransferase (ALT), 5′-nucleotidase (5′-NT), and γ-glutamyltransferase (GGT) were measured. The albumin/globulin ratio (A/G) was calculated as albumin/(total protein-albumin).

^{1}H HR MAS NMR Spectroscopy of Intact Liver. The liver tissue samples were analyzed by ^{1}H MAS NMR spectroscopy at 400.13 MHz using a Bruker AV-400 spectrometer (Bruker Biospin, Rheinstetten, Germany) equipped with a high-resolution magic-angle-spinning (HRMAS) probe head with a magic angle field gradient coil. Each sample (approximately 12 mg) was rinsed in saline D_2O, placed in a 4 mm zirconium oxide rotor, and spun at 4 kHz. To avoid sample degradation, the NMR spectra were acquired at an external temperature of 276 K as measured by a Bruker VTU 3000 temperature control unit. In total, 512 transients were collected into 16K data points using a spectral width of 8 kHz and a standard 1D pulse sequence for solvent presaturation suppression (RD-90°-t_1-90°-t_m-90°-acquire data) with irradiation at the water frequency during the relaxation delay, RD, of 2 s and during the mixing time, t_m, of 100 ms. The chemical shifts were referenced to that of the anomeric proton resonance of α-glucose (δ 5.233).

^{1}H NMR Spectroscopy of Blood Plasma. The plasma samples were prepared for NMR analysis by mixing 150 μL of plasma with 350 μL of saline (0.9% w/v NaCl in a mixture of 10% v/v D_2O and 90% v/v H_2O). The samples were analyzed by ^{1}H NMR spectroscopy at 600.13 MHz using a Bruker AMX-600 spectrometer. The data were acquired at a nominal 310K with 64 transients being collected into 64K data points using the standard 1D pulse sequence with solvent presaturation suppression given above. A spectral width of 10 kHz and an acquisition time per scan of 3.28 s were used. Water suppression irradiation was applied during RD (3 s) and during the mixing time, t_m, of 100 ms. Chemical shifts were referenced to that of the anomeric proton resonance of α-glucose taken as δ 5.233. Standard Carr−Purcell−Meiboom−Gill (CPMG) spin−echo spectra were also acquired for 128 transients using the pulse sequence (RD-90°-(τ-180°-τ)$_n$-acquire) with a total spin−spin relaxation delay, $2n\tau$, of 87.8 ms. The CPMG spectrum emphasizes resonances from metabolites having unconstrained molecular motion (short rotational correlation time) with the resonances of high molecular weight compounds being attenuated via T_2 relaxation in the $2n\tau$ spin−spin relaxation delay period.[26]

^{1}H NMR Spectroscopy of Urine. Urine samples were prepared by mixing 200 μL of phosphate buffer (81:19 v/v mixture of 0.2 M Na_2HPO_4 and 0.2 M NaH_2PO_4; pH 7.4) with 400 μL of urine. The urine−buffer mixture was left to stand for 10 min at room temperature and then centrifuged at 13 000 rpm for a further 10 min. The clear supernatant (500 μL) was then pipetted into a 5 mm NMR tube together with 50 μL of TSP/D_2O. The former served as a chemical shift reference (δ 0.0), and the latter served as a field-frequency lock. The urine samples were analyzed at 303 K by ^{1}H NMR spectroscopy at 600.13 MHz using a Bruker AMX-600 spectrometer. In total, 64 transients were collected into 64K data points using the standard 1D pulse sequence with solvent presaturation suppression as given above and with irradiation at the water frequency during RD (3 s) and during the mixing time, t_m, of 100 ms.

Multivariate Statistical Data Analysis. Fourier transformed ^{1}H NMR spectra were manually phased and baseline-corrected using XWINNMR 3.5 (Bruker Biospin, Rheinstetten, Germany).

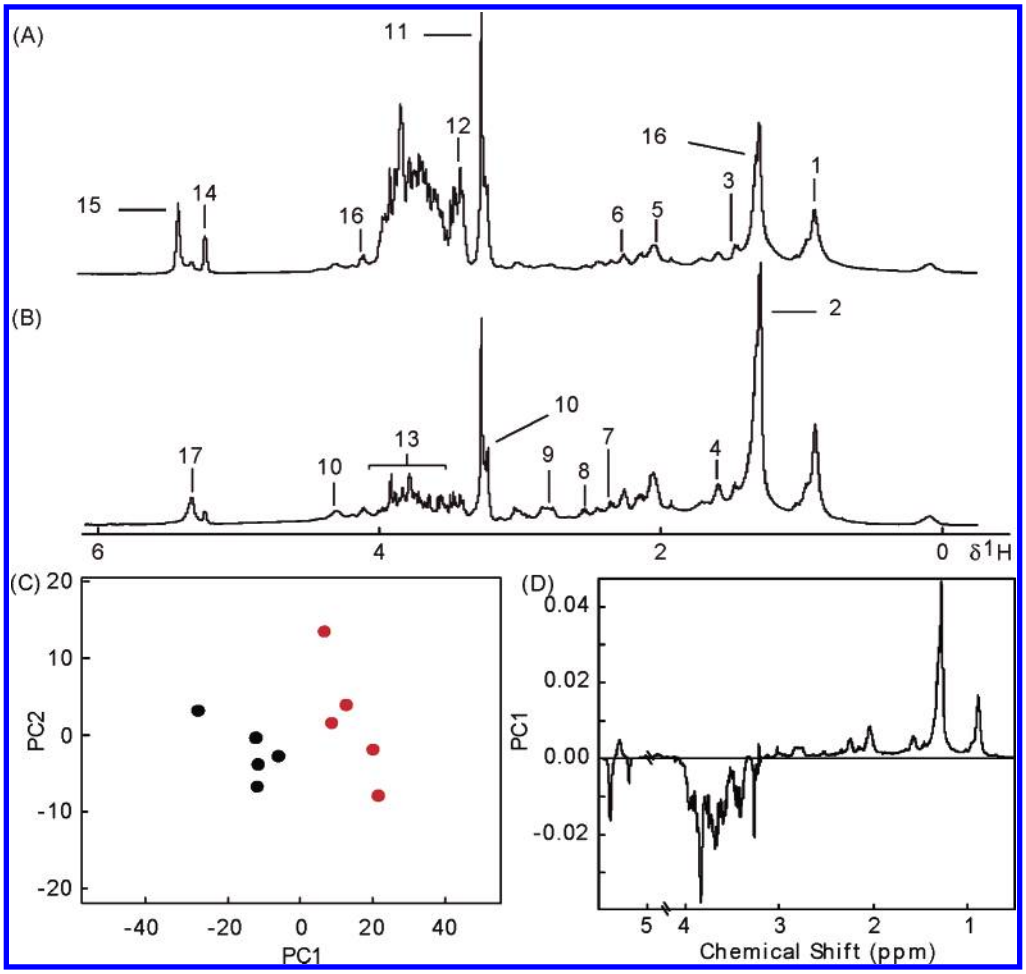

Figure 1. Effects of allyl formate hepatotoxicity as visualized using ^{1}H MAS NMR spectroscopy of intact rat liver. (A) Control liver; (B) liver from an allyl formate-dosed animal. All spectra are from animals sampled on day 2. (C) PCA scores plot (first two PCs) of the ^{1}H MAS NMR spectra of day 2 liver samples from allyl formate-dosed (red circles) and control (black circles) rats, and (D) the corresponding first component loadings plot. Key to numbering in Table 1.

By the use of an in-house-developed MATLAB routine (Olivier Cloarec, unpublished), the MAS NMR and plasma NMR spectra were reduced to 30 999 data points over the range of δ 0.2−8.6 after removal of the water resonance region (δ 4.5−5.0). The urine NMR spectra were reduced to 26 999 data points over the range of δ 0.5−9.0 after removing the water and urea resonance region (δ 4.5−6.4). These data were scaled prior to chemometrics to give the same total integration value (100%) for each spectrum (biofluid or liver). While such scaling is standard practice, it means that the output of the subsequent multivariate statistical analyses must be interpreted with caution with any changes being relative to the total spectral integration rather than absolute. Furthermore, a large increase, for instance, in one component could cause apparent relative decreases in others.

Principal Component Analysis (PCA) with mean centering was carried out on each type of NMR data separately using the SIMCA-P 10.5 software (Umetrics, Umeå, Sweden) in order to discern the presence of inherent similarities of spectral profiles. Partial Least Squares (PLS) analysis with mean centering was also carried out in order to investigate the possibility of a correlation between the changes observed in the plasma and the changes observed in the liver. PLS is designed to relate two data matrices, X (in this case liver NMR) and Y (in this case plasma NMR), with each other by means of a linear multivariate model. It provided a means to model the liver NMR and plasma NMR data matrices as well as to identify input and process variables (liver NMR) that are responsible for the change in the output variables (plasma NMR) with the aim of maximizing the correlation between liver and plasma data. O-PLS-DA with unit variance scaling was carried out on concatenated liver and plasma NMR data as well as on urine NMR data using the method described previously by Cloarec et al.[27] in order to remove confounding variation and focus solely on the effects of AF. The O-PLS-DA approach involved decomposing the variation in X (the NMR data) into three parts, the first being the variation in X related to Y (the class variable), and the last two containing the specific systemic variation in X and residual, respectively.[27] The contribution of each metabolite to sample classification is interpreted using the loadings with back-scaling transformation as well as weight of the variable contributing to the discrimination in the models.[27] The colors projected onto the spectrum indicate the correlation of NMR data with the class of treatment with red corresponding to a high correlation and blue indicating no correlation with sample class, as calculated from the correlation matrix with back-transformation using the covariance in order to preserve the original spectral data structure. The results from the NMR and multivariate analysis were then compared with those from histopathology and clinical chemistry to provide a compre-

Table 1. ^{1}H Chemical Shift Assignment of the Metabolites in Liver, Plasma, and Urine Perturbed after Treatment with Allyl Formate[a]

biological matrices	key[b]	metabolites	moieties	δ ^{1}H (ppm) and multiplicity
liver	1	lipids	CH_3	0.89(m)
	2	lipids	$(CH_2)n$	1.27(m)
	3	alanine	CH_3	1.47(d)
	4	lipids	$CO-CH_2-CH_2$	1.61(m)
	5	lipids	$CH_2-C=C$	2.0(m)
	6	lipids	$CH_2-C=O$	2.3(m)
	7	glutamate	CH_2	2.36(m)
	8	glutamine	CH_2	2.44(m)
	9	lipids	$=C-CH_2-C=$	2.78(m)
	10	choline	$N-(CH_3)_3$, αCH_2	3.20(s), 4.05(t)
	11	TMAO	$N-(CH_3)_3$	3.27(s)
	12	taurine	$S-CH_2$	3.40(t)
	13	glucose/glycogen/α-H amino acids	ring protons/α-CH	3.35−4.00
	14	α-glucose	CH	5.23(d)
	15	glycogen	CH	5.38−5.45
	16	lactate	αCH, βCH_3	4.11(q), 1.32(d)
	17	unsaturated lipids	$-CH=CH-$	5.3(m)
plasma	1, 2	leucine	γCH_3,δCH_3	0.91(d), 0.94(d)
	3	valine	γCH_3	0.98(d)
	4, 5	isoleucine	γCH_3,δCH_3	0.99(t), 1.02(d)
	6	U_1	−	1.06−1.07
	7	isobutyrate	CH_3	1.13(d)
	8	acetoacetate	CH_3	2.29(s)
	9	lipid	$CO-CH_2$	2.23(m)
	10	pyruvate	CH_3	2.41(s)
	11	glutamine	γCH_2	2.44(m)
	12	lipids (VLDL/LDL)	$-CH_3$	0.87 (t)
	13	lipids (VLDL/LDL)	$-CH_2-$	1.29(m)
	14	lactate	αCH, βCH_3	4.11(q), 1.32(d)
	15	lipids (VLDL/LDL)	$-(CH_2)_n$	1.57(m)
	16, 17	arginine/lysine	βCH_2, γCH_2	1.89(m), 1.72(m)
	18	*N*-acetyl glycoproteins	CH_3	2.04 (s)
	19	methionine	$S-CH_3$	2.13(s)
	20	creatine	$N-CH_3$, CH_2	3.03(s), 3.92(s)
	21	choline	$N-(CH_3)_3$	3.20(s)
	22	unsaturated lipids	$-CH=CH-$	5.3(m)
	23	phenylalanine	ring-CH	7.40(m), 7.33(m), 7.35(m)
	24	3-D-hydroxybutyrate	γCH_3	1.20(d)
	25	alanine	CH_3	1.46(d)
	26	acetate	CH_3	1.91(s)
	27	citrate	CH_2(1/2), CH_2(1/2)	2.55(d), 2.65 (d)
	28	taurine	$S-CH_2$	3.40(t)
	29	glucose/amino acids resonances	ring protons/α-CH	3.40−4.00
	30	TMAO	$N-(CH_3)_3$	3.27(s)
	31	α-glucose	CH	5.23(d)
	32	tyrosine	CH, CH	7.16(m), 6.87(m)
urine	1	*N*-acetyl glycoproteins	CH_3	2.04 (s)
	2	succinate	CH_2	2.42(s)
	3,6	2-oxoglutarate	CH_2, CH_2	2.45(t), 3.01(t)
	4	citrate	CH_2(1/2), CH_2(1/2)	2.55(d), 2.65(d)
	5	dimethylglycine	CH_3	2.93(s)
	7	TMAO	$N-(CH_3)_3$	3.27(s)
	8,9	taurine	$N-CH_2$, $S-CH_2$	3.26(t), 3.40(t)
	10	creatine	$N-CH_3$, CH_2	3.03(s), 3.92(s)
	11	hippurate	αCH, mCH, pCH, oCH	3.97(d), 7.55(t), 7.64(t), 7.84(d)
	12	creatinine	$N-CH_3$, CH_2	3.04(s), 4.05(s)
	13	phenylacetylglycine (PAG)	CH, CH, CH	7.35(d), 7.35(t), 7.42(t)

[a] Keys: s: singlet, d: doublet, t: triplet, q: quartet, m: multiplet, dd: doublet of doublet, U_1, unidentified. [b] Numbers correspond with metabolites position on NMR spectra in Figures.

hensive analysis of time-related toxic effects and to allow characterization of key metabolic events during the toxic insult.

Quantitation of Components of ^{1}H NMR Spectra. Selected urinary components were quantified relative to creatinine and allantoin. Plasma tyrosine was quantified by reference to the clinical chemistry values for glucose. Quantitation of liver components is less certain, but spectral changes relating to certain components were confirmed by rerunning samples with a weighed piece of silicone rubber added as an internal standard.

Results and Discussion

Histopathology and Clinical Chemistry. Histopathology revealed periportal to diffuse lobular haemorrhagic coagulative liver necrosis in all AF-dosed animals sampled on day 2 with one animal showing mild necrosis, two animals showing moderate necrosis, and two animals showing severe necrosis. All AF-dosed animals sampled on day 8 showed multifocal chronic postnecrotic hepatic inflammation. In the AF-dosed animals sampled on day 2, plasma levels of ALT, AST, TBA,

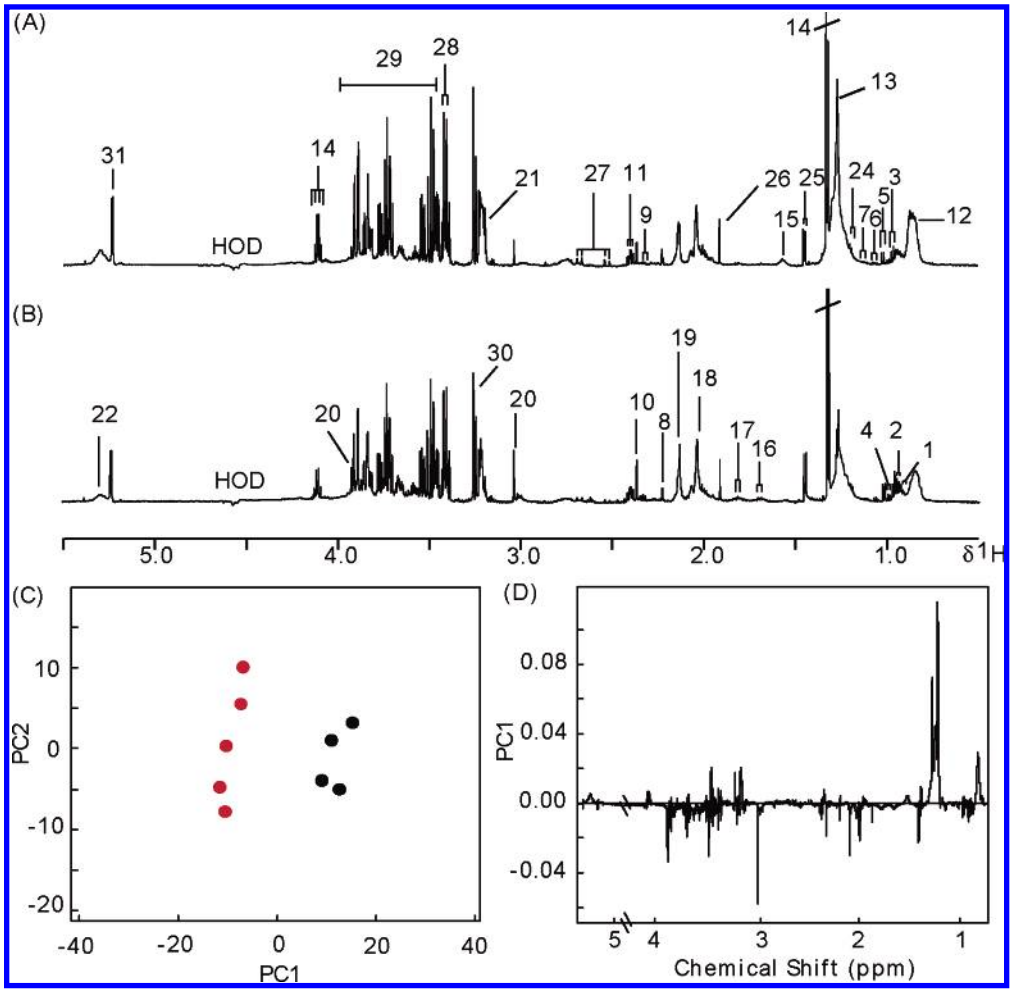

Figure 2. Effects of allyl formate hepatotoxicity as visualized using CPMG ^{1}H NMR spectroscopy of rat plasma. (A) Control plasma; (B) plasma from an allyl formate-dosed animal. All spectra are from animals sampled on day 2. (C) PCA scores plot (first two PCs) of the ^{1}H NMR CPMG spectra of day 2 plasma samples from allyl formate-dosed (red circles) and control (black circles) rats, and (D) the corresponding first component loadings plot. Note: One control sample was excluded due to imperfect water suppression. Key to numbering in Table 1.

and GGT were increased, and the levels of plasma triglycerides, albumin, and TP were decreased in comparison to the day 2 controls. On day 2, the average AF-induced decrease in plasma triglycerides was 54%.

Characterization of AF Effects on the Liver Metabolite Profiles. A typical ^{1}H HRMAS NMR spectrum of intact liver tissue from a control rat acquired using the standard 1D pulse sequence for solvent suppression is shown in Figure 1A. The main peaks arise from glucose, glycogen, TMAO, and lipid moieties, mainly triglycerides and phospholipids (Table 1).[28,29] A similar pattern of changes occurred in all the AF-dosed animals sampled on day 2, with relative increases in lipid signals at δ 0.90 and δ 1.30, relative decreases in the glucose resonances in the region of δ 3.40−4.00 and δ 5.23, and relative decreases in the glycogen signals at δ 5.42 and δ 3.80 (Figure 1B). Visual inspection of these spectra revealed that the extent of the changes to the lipid peaks broadly reflected the extent of the necrosis identified by histopathology with 2/5 animals showing the smallest changes in these NMR signals, one showing intermediate change in lipids, and the remaining two showing the largest changes in total lipid intensity. In contrast, the AF-dosed animals sampled at day 8 showed only minor changes compared to controls. A PCA scores plot derived from the day 2 data shows two clusters of samples relating to control and AF-dosed animals with no overlap between the two groups (Figure 1C). The corresponding loadings plot (Figure 1D) confirmed the relative spectral changes identified above.

Characterization of AF Effects on the Plasma Metabolite Profiles. A typical ^{1}H CPMG NMR spectrum of a control blood plasma is shown in Figure 2A and shows resonances from a range of abundant low molecular weight metabolites with little contribution from the high molecular weight moieties (Table 1). Most resonances have been assigned previously, and the compounds detected include lipoproteins, both α- and β-anomers of glucose, and various low molecular weight metabolites such as lactate, pyruvate, valine, and alanine.[28,29] Clear differences from controls were observed in the day 2 plasma spectra of the AF-dosed animals with marked increases in the creatine signals at δ 3.04 and δ 3.92. Additionally, 4/5 animals showed an increase in tyrosine, and 4/5 animals showed an altered lipoprotein profile (Figure 2B). No significant changes were observed in the day 8 plasma profiles of the AF-dosed animals as compared to controls. A PCA scores plot (Figure 2C) derived from the day 2 ^{1}H NMR plasma spectra shows two distinct clusters relating to control and AF-dosed animals. From the PC loadings (Figure 2D), the metabolites discriminating be-

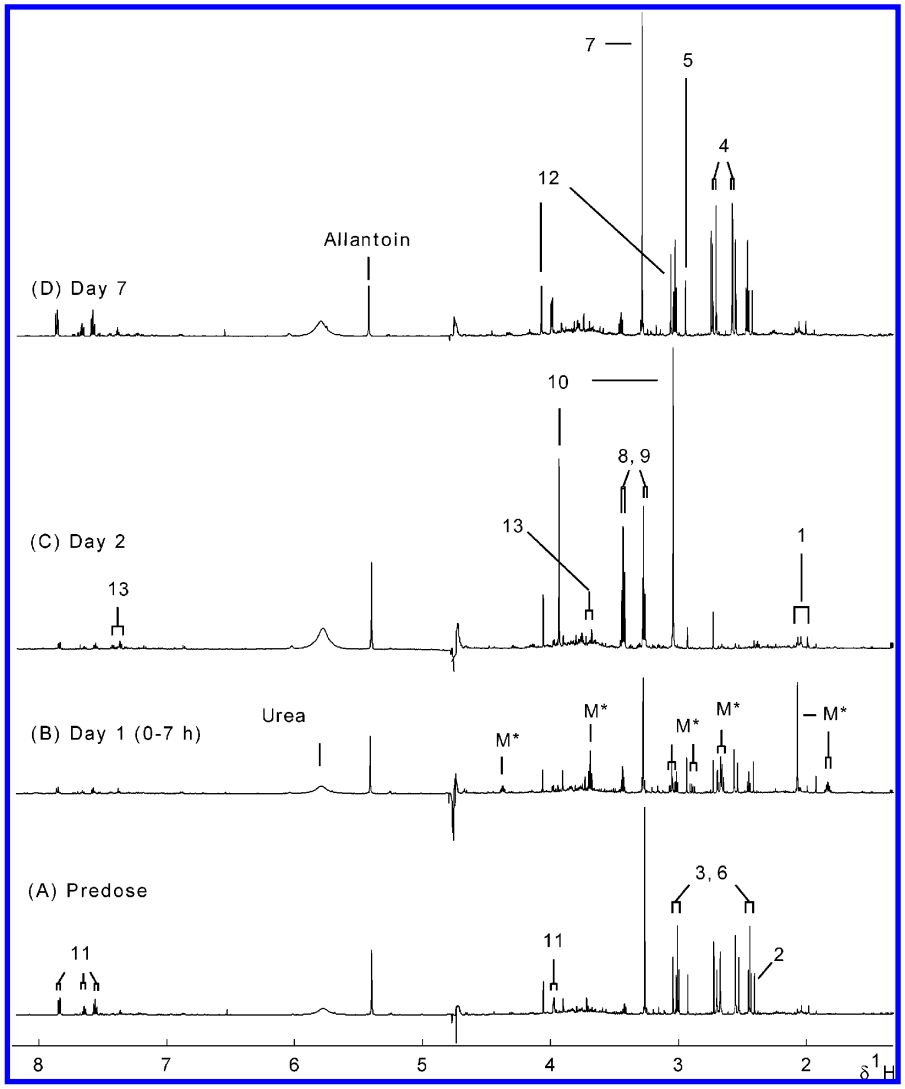

Figure 3. A series of 600 MHz ^{1}H NMR spectra (δ 0.0−9.0) of urine from an AF-dosed animal at (A) predose, (B) day 1, (C) day 2, and (D) day 7. Key: M* is 3-HPMA, a metabolite of AF. Key to numbering in Table 1.

tween the control and dosed animals include lipids (lower in dosed animals) and acetate, N-acetylated compounds, pyruvate, and creatine, and tyrosine (all higher in dosed animals).

The Effects of AF on Urinary Metabolite Profiles. The effects of AF treatment on endogenous urinary metabolites were assessed using the sequence of daily urine samples from animals euthanized at day 8. AF induced marked changes in the endogenous urinary metabolites, and the overall pattern of changes was strongly suggestive of hepatotoxicity.[11,14,17] The dominant changes observed were increases in creatine, taurine, and phenylacetylglycine (PAG), and decreases in succinate, citrate, 2-oxoglutarate, TMAO, and hippurate (Figure 3). 3-Hydroxypropylmercapturic acid (3-HPMA), an *N*-acetyl cysteine conjugate derived from AF, was also detected in day 1 (0−7 h) and day 1 (7−24 h) urine samples from the AF-dosed group. The presence of 3-HPMA in the urine is consistent with the metabolism of AF to toxic acrolein and the formation of a glutathione conjugate.[30−33]

To investigate the time course of metabolic events in the rat following dosing of allyl formate, mean PC scores trajectories were calculated from the first two PCs of the normalized ^{1}H NMR spectra of urine, describing 66% of the total variance in the original data. The day 1 data were excluded from this analysis because of the presence of 3-HPMA. In the mean trajectory analysis, the degree of movement away from the control space indicates the magnitude of the metabolic effect after AF treatment. Maximum effects were reached at day 3 with apparent recovery by day 6. The modeled metabolic evolution comprised three distinct phases. In phase one, corresponding to movement to the day 2 time point, the trajectory of the urine sample coordinates moved away from the predose position along the first component. Thereafter, in phase two, corresponding to movement to the day 3 time point, the trajectory changes direction moving away from the origin along the second component. Finally, in phase three, corresponding to movement to the day 7 time point, the trajectory returned to within the predose space indicating recovery. Focusing, in a further PCA, on the urinary changes observed at day 2, a PC scores plot shows two clusters of samples relating to control and AF-dosed animals (Figure 4A). The corresponding coefficients plot calculated from O-PLS-DA (Figure 4B) indicated that urine from the AF-dosed rats exhibited lower levels of hippurate, 2-oxoglutarate, succinate, citrate, and trimethylamine-*N*-oxide (TMAO) and higher levels of phenylacetylglycine (PAG), *N*-acetyl glycoproteins, creatine, and taurine than the urine from the controls.

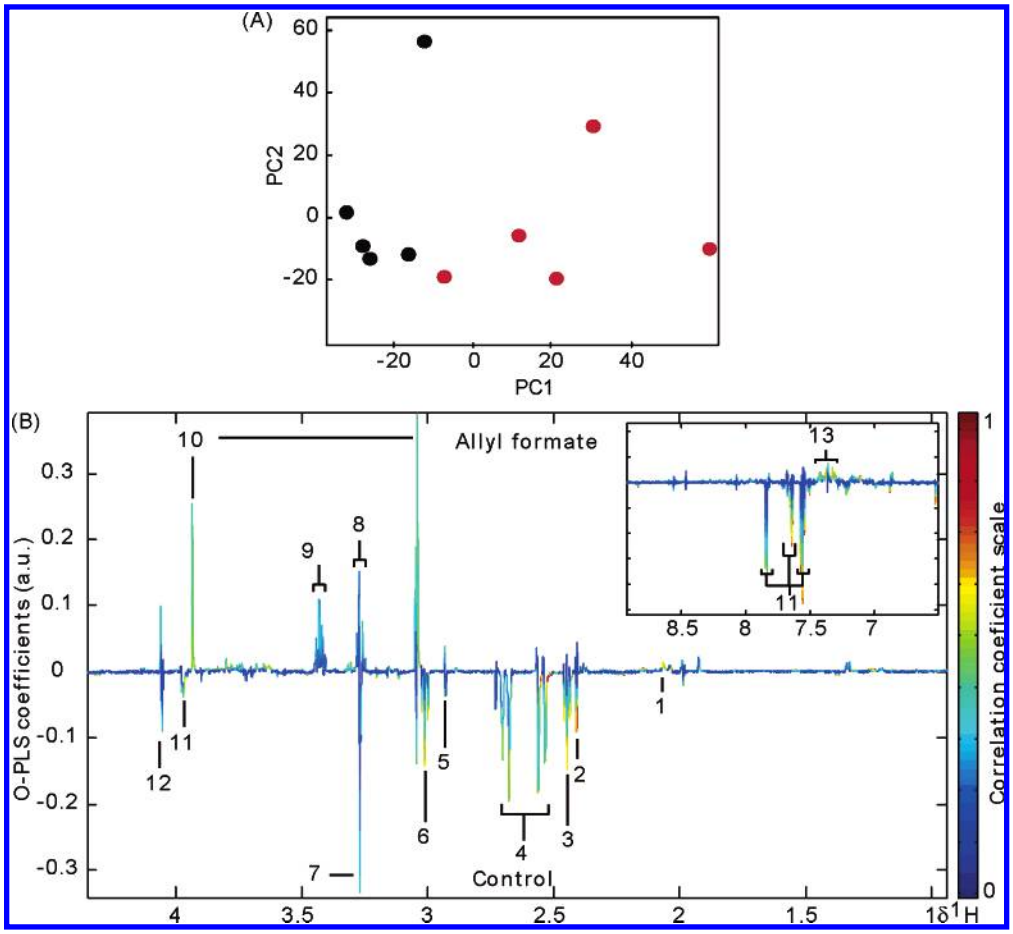

Figure 4. (A) PCA scores plot (first two PCs) derived from ^{1}H NMR spectra of day 2 urine samples from allyl formate-dosed (red circles) and control rats (black circles), and (B) O-PLS-DA coefficients related to the urinary NMR-based discrimination of control and allyl formate-dosed animals on day 2 ($Q^2Y = 64.1\%$). The aromatic spectral region (δ 6.8−8.8) is shown in the inset. Key to numbering in Table 1.

Table 2. The AF-induced Changes Observed on day 2 in the Liver, Blood Plasma, and Urine[a]

allyl formate (75 mg/kg)							
		liver NMR		plasma NMR		urine NMR	
histopathology	plasma chemistry	metabolite (*)	correlation coefficients	metabolite (*)	correlation coefficients	metabolite (*)	correlation coefficients
Periportal to diffuse lobular haemorrhagic coagulative necrosis with various degree of severity.	AST: ↑ (***)	Glycogen (16) ↓	−0.97	VLDL (13) ↓	−0.99	Hippurate (11) ↓	−0.81
	ALT: ↑ (***)	Glucose (15) ↓	−0.96	LDL (12) ↓	−0.99	Succinate (2) ↓	−0.76
	TBA: ↑ (***)	Lipids (9) ↑	0.91	*N*-acetyl glycoproteins (18) ↑	0.94	*N*-acetyl glycoprotein (1) ↑	0.75
	GGT: ↑ (***)	Lipids (5) ↑	0.89	Methionine (19) ↑	0.94	2-oxoglutarate (3) ↓	−0.73
	Triglycerides: ↓ (***)	Taurine (13) ↓	−0.89	Isoleucine (1) ↑	0.91	PAG (13) ↑	0.73
	Albumin: ↓ (**)	Alanine (3) ↑	0.88	Unsaturated lipids (22) ↓	−0.85	Citrate (4) ↓	−0.65
	TP: ↓ (***)	Lipids (4) ↑	0.77	Creatine (20) ↑	0.84	Creatine (10) ↑	0.61
		Lipids (18) ↑	0.73	Arginine/Lysine (17) ↑	0.83	TMAO (7) ↓	−0.54
		'Choline' (11) ↑	0.59	Glutamine (11) ↑	0.81	Taurine (9) ↑	0.43
		Lactate (17) ↑	0.52	'Choline' (21) ↓	−0.78		
		TMAO (12) ↓	−0.5	Phenylalanine (23) ↑	0.77		
		Lipids (2) ↑	0.36	Tyrosine (32) ↑	0.72		
		Lipids (1) ↑	0.018	Pyruvate (10) ↑	0.66		
				Leucine (3) ↑	0.58		
				Acetate (28) ↑	0.53		
				Acetoacetate (8) ↑	0.53		
				3-D-hydroxybutyrate (26) ↑	0.52		

[a] Key: Statistics, significant difference at (**) $p < 0.01$, and (***) $p < 0.001$ confidence level; * numbers correspond to the metabolite peak positions on NMR spectra in Figures; the correlation coefficients shown are based on O-PLS-DA analysis of a two-class model (control and dosed), positive value indicate an increase of the metabolite in the dosed group (also indicated by an up-arrow). 'Choline' indicates choline or choline-containing compounds such as phosphatidylcholine.

Integrated Analysis of the Effect of Allyl Formate in the Rat. All the analyses performed (histopathology, plasma chemistry, liver NMR, plasma NMR, and urine NMR) revealed substantial AF-induced changes and a high degree of recovery by the end of the study. The changes observed on day 2 are summarized in Table 2. Substantial interanimal variation in the

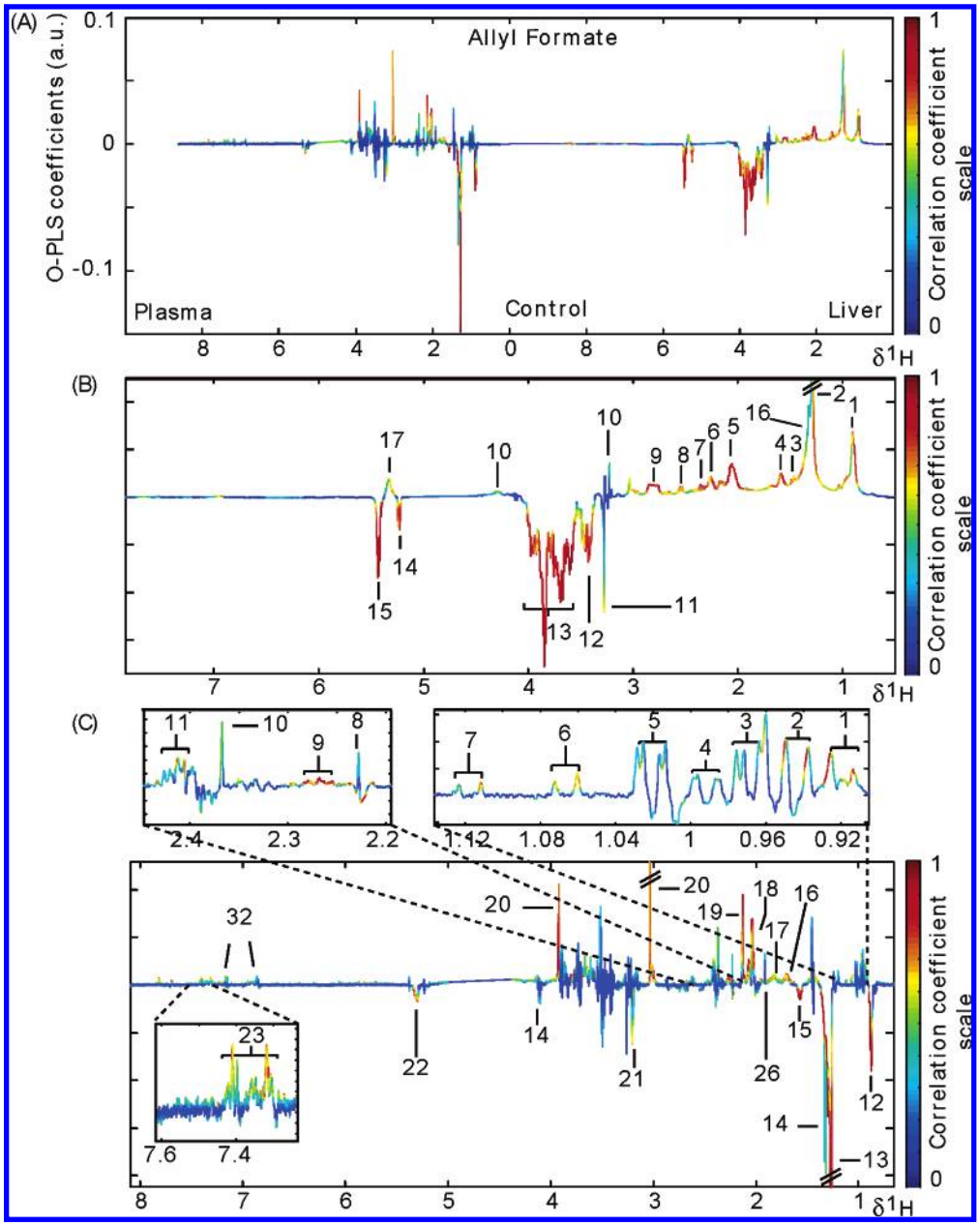

Figure 5. (A) O-PLS-DA coefficients related to the discrimination between allyl formate-dosed and control rats in concatenated ^{1}H NMR spectra of day 2 liver and plasma samples ($Q^2Y = 90.7\%$). (B) An expansion of the coefficients relating to the liver data. (C) Expansions of the coefficients relating to the plasma data. Key to numbering in Table 1.

extent of the AF-induced changes was seen in all the analyses performed (i.e., by histopathology; by clinical chemistry; and in the NMR analysis of the urine, plasma, and liver). Interestingly, the animals showing the greatest degree of liver necrosis and the biggest increases in plasma AST and ALT also showed the biggest relative increases in liver lipids as observed by MAS NMR. Thus, these findings indicate that the NMR analysis of the liver is detecting a toxicologically relevant change (i.e., lipidosis) that was not revealed by histopathology. The O-PLS-DA coefficients of the concatenated day 2 liver and plasma NMR data (Figure 5) indicate AF-induced hepatic lipidosis with significant increases in liver lipids and lower levels of hepatic glucose, glycogen, taurine, and TMAO. In addition, the coefficients also indicate increases in liver alanine and in choline-containing compounds. The O-PLS-DA coefficients also indicate reduced levels of lipids and choline-containing compounds in the plasma of AF-dosed animals in comparison with the controls, together with increased levels of creatine, N-acetylated compounds, acetate, acetoacetate, and 3-D-hydroxybutyrate. The O-PLS-DA also indicated AF-induced increases in the levels of plasma amino acids including lysine, isoleucine, leucine, phenylalanine, glutamine, tyrosine, and methionine in decreasing order of influence on class separation.

The indicated AF-induced increase in plasma tyrosine was confirmed and suggests impaired protein synthesis within the liver where tyrosine is normally converted to *p*-hydroxyphenylpyruvate through the action of tyrosine aminotransferase (TAT), which is an unusually short-lived enzyme with a half-life of about 2.5 h.[34] Thus, AF-induced impairment of hepatic protein synthesis could rapidly lead to TAT depletion and to consequent increases in tyrosine in the liver and blood. The indicated increases in the levels of some other amino acids, in

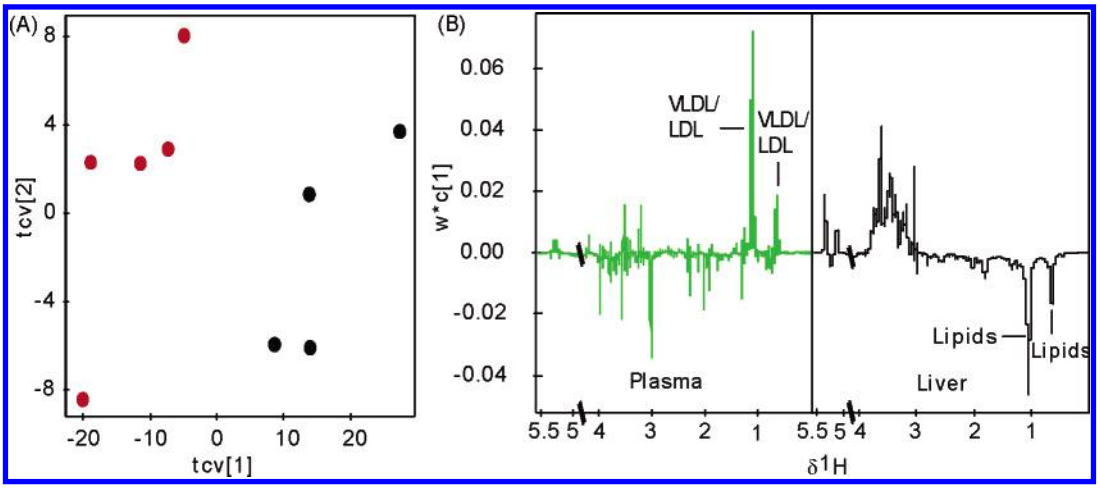

Figure 6. (A) A scores plot (first two PCs) derived from the PLS analysis that was used to inter-relate the variation in the NMR spectra of the day 2 liver and plasma samples from allyl formate-dosed (red circles) and control rats (black circles), and (B) the corresponding loadings plots showing the correlation between liver lipids and plasma lipids.

particular isoleucine and leucine, are also suggestive of perturbed protein synthesis.

Reduced urinary excretion of the citric acid cycle intermediates, succinate, citrate, and 2-oxoglutarate, is a common response to hepatotoxins and suggests perturbed energy metabolism. The observed decreases in liver glycogen and glucose suggest increased energy demand, with possible increases in glycogenolysis and glycolysis, which is consistent with previous studies indicating that AF and acrolein cause severe depletion of hepatic ATP and inhibition of mitochondrial respiration.[35−44]

PLS cross-correlation of the variation in the day 2 liver and plasma NMR data (Figure 6A) showed two clusters of samples relating to control and AF-dosed animals. The corresponding loadings plot (Figure 6B) revealed an AF-induced increase in liver triglycerides that appeared to correlate to a decrease in plasma lipids, which could indicate reduced lipid transport from the liver to the plasma, as in the case of the changes induced in rats by ethionine where ATP depletion leads to impaired protein synthesis and to a subsequent increase in liver triglycerides.[45,46]

In the present study, AF-induced decreases in TMAO were observed in both liver and urine. A major route of biosynthesis of TMAO starts from the degradation of dietary choline, which is first metabolized to trimethylamine (TMA) by the enzymes of the gut microflora.[47,48] The TMA produced is then normally oxidized to TMAO by the flavin monooxygenase system of the liver, and TMAO is subsequently excreted in the urine.[47−51] Thus, the observed TMAO changes in AF-dosed animals could potentially reflect a variety of factors such as reduced food intake, disruption of intestinal bacteria, or disruption of liver function. The possibility of an AF-induced effect on the gut microflora is also suggested by the urinary changes in hippurate and phenylacetylglycine (PAG), since their precursors, benzoic acid and phenylacetic acid, are produced by bacterial metabolism in the intestine.[52−59] Furthermore, changes in urinary hippurate and PAG have been previously linked to the effects of xenobiotics on the intestinal microfloral metabolism of plant phenolics.[59] However, as with TMAO, the liver also has a major role in the production of hippurate and PAG, with glycine conjugation of the precursor acids being performed by the hepatic mitochondria.[55,57] Thus, AF-induced disruption of liver function, and in particular of mitochondrial function, could potentially be involved in the observed decrease in urinary hippurate.[55] However, the observed increase in urinary PAG cannot be similarly attributed to mitochondrial impairment, and one possibility is that glycine conjugation proceeds normally, but an increase in phenylacetic acid production leads to a reduction in the amount of glycine that is available to conjugate with benzoic acid.[52]

Conclusion

The present study demonstrates the benefit of metabonomic analysis of multiple biological compartments with each sample type giving a different insight into the effects of the toxin. In particular, the integrated NMR analysis of both liver and plasma samples, collected at the same point in the study, 1 day after AF-dosing, points to depletion of hepatic energy reserves, to impairment of hepatic protein synthesis, and to hepatic lipidosis arising from a consequent inability to transport lipids from the liver to the plasma.

Abbreviations: 3-HPMA, 3-hydroxypropyl mercapturic acid; AF, allyl formate; CPMG, Carr−Purcell−Meiboom−Gill; GSH, glutathione; MAS, magic angle spinning; NMR, nuclear magnetic resonance; O-PLS-DA, orthogonal signal correction-Projection to latent structure-discriminant analysis;PLS, partial least squares; PAG, phenylacetylglycine; TMAO, trimethylamine-*N*-oxide; TSP, sodium 3-trimethylsilyl-[2,2,3,3-$^2H_4$]-1-propionate.

Acknowledgment. The authors thank Dr. O. Cloarec for allowing us to use MATLAB scripts to process NMR data and for considerable guidance. The authors also gratefully acknowledge the facilities and assistance provided by the ULIRS NMR Service at Queen Mary and Westfield College, London. The UK Department for Education and Skills (Overseas Research Scholarship Department) and Pfizer Global Research and Development, Sandwich, U.K., are acknowledged for financial support to I.K.S.Y. The staff of Pfizer Global Research and Development (Amboise, France) are acknowledged for conducting the animal work, for performing the clinical chemistry and histopathological analyses, and for providing samples for NMR.

References

(1) Nicholson, J. K.; Lindon, J. C.; Holmes, E. *Xenobiotica* **1999**, *29*, 1181−1189.

(2) Nicholson, J. K.; Connelly, J.; Lindon, J. C.; Holmes, E. *Nat. Rev. Drug Discovery* **2002**, *1*, 153−161.
(3) Nicholson, J. K.; Wilson, I. D. *Nat. Rev. Drug Discovery* **2003**, *2*, 668−676.
(4) Nicholson, J. K.; Holmes, E.; Lindon, J. C.; Wilson, I. D. *Nat. Biotechnol.* **2004**, *22*, 1268−1274.
(5) Craig, A.; Sidaway, J.; Holmes, E.; Orton, T.; Jackson, D.; Rowlinson, R.; Nickson, J.; Tonge, R.; Wilson, I.; Nicholson, J. *J. Proteome Res.* **2006**, *5*, 1586−1601.
(6) Plumb, R. S.; Stumpf, C. L.; Gorenstein, M. V.; Castro-Perez, J. M.; Dear, G. J.; Anthony, M.; Sweatman, B. C.; Connor, S. C.; Haselden, J. N. *Rapid Commun. Mass Spectrom.* **2002**, *16*, 1991−1996.
(7) Plumb, R. S.; Stumpf, C. L.; Granger, J. H.; Castro-Perez, J. M.; Haselden, J. N.; Dear, G. J. *Rapid Commun. Mass Spectrom.* **2003**, *17*, 2632−2638.
(8) Tomlins, A. M.; Foxall, P. J. D.; Lindon, J. C.; Lynch, M. J.; Spraul, M.; Everett, J. R.; Nicholson, J. K. *Anal. Commun.* **1998**, *35*, 113−115.
(9) Cheng, L. L.; Wu, C.; Smith, M. R.; Gonzalez, R. G. *FEBS Lett.* **2001**, *494*, 112−116.
(10) Nicholls, A. W.; Holmes, E.; Lindon, J. C.; Shockcor, J. P.; Farrant, R. D.; Haselden, J. N.; Damment, S. J. P.; Waterfield, C. J.; Nicholson, J. K. *Chem. Res. Toxicol.* **2001**, *14*, 975−987.
(11) Waters, N. J.; Waterfield, C. J.; Farrant, R. D.; Holmes E.; Nicholson, J. K. *J. Proteome Res.* **2006**, *5*, 1448−1459.
(12) Andrew, E. R.; Eades, R. G. *Nature* **1959**, *183*, 1802.
(13) Bollard, M. E.; Garrod, S.; Holmes, E.; Lindon, J. C.; Humpfer, E.; Spraul, M.; Nicholson, J. K. *Magn. Reson. Med.* **2000**, *44*, 201−207.
(14) Coen, M.; Lenz, E. M.; Nicholson, J. K.; Wilson, I. D.; Pognan, F.; Lindon, J. C. *Chem. Res. Toxicol.* **2003**, *16*, 295−303.
(15) Garrod, S.; Humpher, E.; Connor, S. C.; Connelly, J. C.; Spraul, M.; Nicholson, J. K.; Holmes, E. *Magn. Reson. Med.* **2001**, *45*, 781−790.
(16) Griffin, J. L.; Williams, H. J.; Sang, E.; Nicholson, J. K. *Magn. Reson. Med.* **2001**, *46*, 249−255.
(17) Waters, N. J.; Holmes, E.; Williams, A.; Waterfield, C. J.; Farrant, R. D.; Nicholson, J. K. *Chem. Res. Toxicol.* **2001**, *14*, 1401−1412.
(18) Beckonert, O.; Monnerjahn, J.; Bonk, U.; Leibfritz, D. *NMR Biomed.* **2003**, *16*, 1−11.
(19) Wang, Y.; Tang, H.; Holmes, E.; Lindon, J. C.; Turini, M. E.; Sprenger, N.; Bergonzelli, G.; Fay, L. B.; Kochhar, S.; Nicholson, J. K. *J. Proteome. Res.* **2005**, *4*, 1324−1329.
(20) Holmes, E.; Nicholls, A. W.; Lindon, J. C.; Ramos, S.; Spraul, M.; Neidig, P.; Connor, S. C.; Connelly, J.; Damment, S. J. P.; Haselden, J.; Nicholson, J. K. *NMR Biomed.* **1998**, *11*, 235−244.
(21) Wang, Y.; Bollard, M. E.; Keun, H. C.; Antti, H.; Beckonert, O.; Ebbels, T. M. D.; Lindon, J. C.; Holmes, E.; Tang, H.; Nicholson, J. K. *Anal. Biochem.* **2003**, *323*, 26−32.
(22) Holmes, E.; Cloarec, O.; Nicholson, J. K. *J. Proteome Res.* **2006**, *5*, 1313−1320.
(23) McManus, J. F.; Cason, J. *J. Exp. Med.* **1950**, *91*, 651−654.
(24) Chiffelle, T. L.; Putt, F. *Stain Technol.* **1951**, *26*, 51−56.
(25) Bowen, R. C. *Ohio J. Sci.* **1968**, *68*, 85−91.
(26) Johnson,, C. S., Jr. *Prog. Nucl. Magn. Reson. Spectrosc.* **1999**, *34*, 203−256.
(27) Cloarec, O.; Dumas, M. E.; Trygg, J.; Craig, A.; Barton, R. H.; Lindon, J. C.; Nicholson, J. K.; Holmes, E. *Anal. Chem.* **2005**, *77*, 517−526.
(28) Nicholson, J. K.; Foxall, P. J.; Spraul, M.; Farrant, R. D.; Lindon, J. C. *Anal. Chem.* **1995**, *67*, 793−811.
(29) Fan, T. W. M. *Prog. Nucl. Magn. Reson. Spectrosc.* **1996**, *28*, 161−219.
(30) Kaye, C. M. *J. Biochem.* **1973**, *134*, 1093−1101.
(31) Alarcon, R. A. *Environ. Res.* **1976**, *12*, 317−326.
(32) Sanduja, R.; Ansari, G. A. S.; Boor, P. J. *J. Appl. Toxicol.* **1989**, *9*, 235−238.
(33) Athersuch, T. J.; Keun, H.; Tang, H.; Nicholson, J. K. *J. Pharm. Biomed. Anal.* **2006**, *40*, 410−416.
(34) Clayton, T. A.; Lindon, J. C.; Everett, J. R.; Charuel, C.; Hanton, G.; Le Net, J. L.; Provost, J. P.; Nicholson, J. K. *Arch. Toxicol.* **2006**, (in press).
(35) Rees, K. R.; Tarlow, M. J. *J. Biochem.* **1967**, *104*, 757−761.
(36) Zollner, H. *Biochem. Pharmacol.* **1973**, *22*, 1171−1178.
(37) Esterbauer, H.; Ertl, A.; Scholz, N. *Tetrahedron* **1975**, *32*, 285−289.
(38) Belinsky, S. A.; Matsumura, T.; Kauffman, F. C.; Thurman, R. G. *Mol. Pharmacol.* **1984**, *25*, 158−164.
(39) Belinsky, S. A.; Badr, M. Z.; Kauffman, F. C.; Thurman, R. G. *J. Pharmacol. Exp. Ther.* **1986**, *238*, 1132−1137.
(40) Farghali, H.; Rossaro, L.; Gavaler, J. S.; Thiel, D. H. V.; Dowd, S. R.; Williams, D. S.; Ho, C. *Biochim. Biophys. Acta* **1992**, *1139*, 105−114.
(41) Fromenty, B.; Pessayre, D. *Pharmacol. Ther.* **1995**, *67*, 101−154.
(42) Pang, J. M.; Zaleski, J.; Kauffman, F. C. *Toxicol. Appl. Pharmacol.* **1997**, *142*, 87−94.
(43) Burcham, P. C.; Fontaine, F. *J. Biochem. Mol. Toxicol.* **2001**, *15*, 309−316.
(44) Sun, L.; Luo, C.; Long, J.; Wei, D.; Liu, J. *Mitochondrion* **2006**, *6*, 136−142.
(45) Waterfield, C. J.; Turton, J. A.; Scales, M. D. C.; Timbrell J. A. *Arch. Toxicol.* **1993**, *67*, 244−254.
(46) Waterfield, C. J.; Westmoreland, C.; Asker, D. S.; Murdock, J. C.; George, E.; Timbrell, J. A. *Arch. Toxicol.* **1998**, *72*, 588−596.
(47) Smith, J. L.; Wishnok, J. S.; Deen, W. M. *Toxicol. Appl. Pharmacol.* **1994**, *125*, 296−308.
(48) Zhang, A. Q.; Mitchell, S. C.; Smith, R. L. *Food Chem. Toxicol.* **1999**, *37*, 515−520.
(49) Gut, I.; Conney, A. H. *Biochem. Pharmacol.* **1993**, *46*, 239−244.
(50) Ziegler, D. M. *Trends Pharmacol. Sci.* **1990**, *11*, 321−324.
(51) Wu, J. T.; Wu, L. H.; Knight, J. A. *Clin. Chem.* **1986**, *32*, 314−319.
(52) Harlow, B.; Sherwin, C. P. *Annu. Rev. Biochem.* **1935**, *4*, 263−278.
(53) James, M. O.; Bend, J. R. *Biochem. J.* **1978**, *172*, 293−299.
(54) Goodwin, B. L.; Ruthven, C. R. J.; Sandler, M. *Biochem. Pharmacol.* **1994**, *47*, 2294−2297.
(55) Gregus, Z.; Fekete, T.; Halaszi, E.; Klaassen, C. D. *Drug Metab. Dispos.* **1996**, *24*, 1347−1354.
(56) Phipps, A. N.; Stewart, J.; Wright, B.; Wilson, I. D. *Xenobiotica* **1998**, *28*, 527−537.
(57) Kasuya, F.; Yamaoka, Y.; Osawa, E.; Igarashi, K.; Fukui M. *Chem.−Biol. Interact.* **2000**, *125*, 39−50.
(58) Gavaghan, C. L.; Nicholson, J. K.; Connor, S. C.; Wilson, I. D.; Wright, B.; Holmes, E. *Anal. Biochem.* **2001**, *291*, 245−252.
(59) Nicholls, A. W.; Mortishire-Smith, R. J.; Nicholson, J. K. *Chem. Res. Toxicol.* **2003**, *16*, 1395−1404.

PR0601584